

Correlated electronic structure of the alternating single-layer bilayer nickelate $\text{La}_5\text{Ni}_3\text{O}_{11}$

Harrison LaBollita^{1,*} and Antia S. Botana²

¹*Center for Computational Quantum Physics, Flatiron Institute,
162 5th Avenue, New York, New York 10010, USA.*

²*Department of Physics, Arizona State University, Tempe, AZ 85287, USA*

The recent discovery of superconductivity under pressure in Ruddlesden-Popper (RP) nickelates has attracted a great deal of attention. Here, using density-functional theory plus dynamical mean-field theory, we study the correlated electronic structure of the latest superconducting member of the family: the alternating single-layer bilayer nickelate $\text{La}_5\text{Ni}_3\text{O}_{11}$. Due to its alternating single-layer and bilayer structural motif, this hybrid RP nickelate exhibits layer-selective physics with the single-layer neighboring a Mott instability, rendering the bilayer the dominant contributor to its low-energy physics, both at ambient and high pressure. The electronic structure of $\text{La}_5\text{Ni}_3\text{O}_{11}$ ultimately resembles that of the bilayer compound $\text{La}_3\text{Ni}_2\text{O}_7$, pointing to the presence of universal features in the family of superconducting RP nickelates. Thus, $\text{La}_5\text{Ni}_3\text{O}_{11}$ provides a new platform to disentangle the key degrees of freedom underlying superconductivity in pressurized RP nickelates, underscoring the central role of the bilayer structural motif.

I. INTRODUCTION

The recent reports of superconductivity in the pressurized bilayer $\text{La}_3\text{Ni}_2\text{O}_7$ [1–3] and trilayer $\text{La}_4\text{Ni}_3\text{O}_{10}$ [4–6] Ruddlesden-Popper (RP) nickelates reinvigorated the field after intensive exploration of the square-planar layered nickelates [7–11]. In the bilayer RP nickelate, superconductivity with a high critical temperature (T_c) ~ 80 K has been experimentally determined in the bulk under pressures above 15 GPa [1–3]. In the trilayer, a T_c of $\sim 20 - 30$ K can be achieved at a similar pressure threshold [4–6]. In both cases, a structural transition concomitant with the onset of superconductivity takes place from an orthorhombic (bilayer) or monoclinic (trilayer) to a tetragonal crystal structure under pressure [6, 12]. This structural transition suppresses the tiltings of the NiO_6 octahedra present at ambient pressure. This series of discoveries established the RP nickelates $\text{R}_{n+1}\text{Ni}_n\text{O}_{3n+1}$ (R = rare earth, n = number of perovskite-like layers along c) [13] as a new family of superconductors. Formal valence counting gives an average Ni $3d$ filling of $d^{7+1/n}$, highlighting the increasingly important role of the $d_{3z^2-r^2}$ (d_{z^2}) orbitals – an aspect that has drawn a plethora of theoretical attention and that introduced new puzzles in the general understanding of superconductivity in the nickelates [14–40].

To shed light on some of the open questions in the RP nickelates, expanding the search for superconductivity to other members of the family has become a promising research direction. In this context, the new series of hybrid RP phases with general chemical formula $\text{R}_{n+1}\text{Ni}_n\text{O}_{3n+1} \cdot \text{R}_{m+1}\text{Ni}_m\text{O}_{3m+1}$ ($n \neq m$) is a prime target [41]. Here, rather than the uniform stacking of perovskite blocks found in RP phases, novel alternating stacking sequences with m and n blocks along c are achieved instead. The

single-layer trilayer ($\text{La}_2\text{NiO}_4 \cdot \text{La}_4\text{Ni}_3\text{O}_{10}$) polymorph of $\text{La}_3\text{Ni}_2\text{O}_7$ ('1313') was the first hybrid RP nickelate to become superconducting under pressure with $T_c \sim 80$ K [42, 43]. More recently, superconductivity was also reported in the single-layer bilayer $\text{La}_2\text{NiO}_4 \cdot \text{La}_3\text{Ni}_2\text{O}_7$ ($\text{La}_5\text{Ni}_3\text{O}_{11}$) hybrid RP ('1212') under pressure [44].

In contrast to the conventional RP nickelates, an orthorhombic phase without tilts has been proposed for both of these hybrid phases at ambient pressure with pressure stabilizing a tetragonal structure [41, 42, 45, 46]. In $\text{La}_3\text{Ni}_2\text{O}_7$ -1313, DFT+DMFT calculations concluded that the single-layer is in a Mott insulating regime with the low-energy physics being dominated by the correlated trilayer block at ambient pressure and at high-pressures [47, 48]. This electronic structure is consistent with recent angle-resolved photoemission spectroscopy (ARPES) measurements at ambient pressure [49]. In contrast, constrained RPA calculations based on the non-magnetic DFT electronic structure showed that the leading pairing instability in both $\text{La}_3\text{Ni}_2\text{O}_7$ -1313 and $\text{La}_5\text{Ni}_3\text{O}_{11}$ -1212 is dominated by the single-layer block [50, 51].

Motivated by the recent report of superconductivity in pressurized $\text{La}_5\text{Ni}_3\text{O}_{11}$ [44], we employ an advanced many-body electronic structure framework based on density-functional theory and dynamical mean-field theory to study the normal-state properties of this material at ambient and high-pressure. Our results reveal layer-selective physics regardless of pressure, with the bilayer block always dominating the low-energy physics. The evolution of the correlated electronic structure in this hybrid RP mimics that of the conventional bilayer RP nickelate. These findings not only identify $\text{La}_5\text{Ni}_3\text{O}_{11}$ -1212 as a new platform for investigating superconductivity in hybrid RP nickelates but also emphasize the relevant role of the bilayer structural architecture in enabling-high T_c superconductivity in the RP nickelate family.

* hlabbollita@flatironinstitute.org

II. THEORETICAL FRAMEWORK

The charge self-consistent combination of density-functional theory (DFT) and dynamical mean-field theory (DMFT), where the Ni sites act as single-site impurity problems is used to analyze the electronic structure of $\text{La}_5\text{Ni}_3\text{O}_{11-1212}$. The DFT part is performed using an all-electron, full-potential framework built on an augmented plane-wave plus local orbital (APW+lo) basis set, as implemented in the WIEN2k code [52] with the local-density approximation (LDA) for the exchange-correlation functional. The basis set size is set by $R_{\text{MT}}K_{\text{max}} = 7$ and muffin-tin radii (in a.u.) of 2.22, 1.80, and 1.60 for La, Ni, O, respectively. Brillouin zone integration is performed on a $7 \times 7 \times 2$ \mathbf{k} -grid. For the DMFT part, local $\text{Ni}(3d)$ orbitals are obtained by projection from the Kohn-Sham (KS) bands in a large energy window spanning $[-10, 5]$ eV around the Fermi level (ε_F) [53, 54]. The Ni sites consist of a five-orbital correlated subspace in which a Slater Hamiltonian governs the interactions parameterized by a Hubbard $U = 10$ eV and Hund's coupling $J_H = 1$ eV. Each inequivalent single-site impurity problem is solved using the continuous-time quantum Monte Carlo in the hybridization expansion as implemented in TRIQS/CTHYB [55, 56]. The fully-localized limit (FLL) form of the double-counting correction is used [57]. Real-frequency data are obtained from Matsubara data via analytic continuation. The local DMFT Green's function is continued using the maximum entropy method [58] to obtain local \mathbf{k} -integrated spectra. The local self-energies are continued using the Padé method to compute both \mathbf{k} -resolved and \mathbf{k} -integrated spectral functions from the Bloch Green's function. A paramagnetic state is enforced in all calculations.

For the structural data, we employ the lattice constants at ambient pressure and at 15 GPa from Ref. 44. The ambient pressure crystal structure is orthorhombic with $Cmmm$ crystal symmetry, while the high-pressure (15 GPa) crystal structure is tetragonal with $P4/mmm$ crystal symmetry. At both pressures, the internal atomic positions are fully relaxed using the VASP code [59–61] within the generalized gradient approximation [62]

III. RESULTS

Crystal structure and DFT picture.— $\text{La}_5\text{Ni}_3\text{O}_{11}$ (referred to as the ‘1212’ RP nickelate) is the $(n, m) = (1, 2)$ member of the hybrid Ruddlesden-Popper series with general chemical formula $\text{La}_{n+1}\text{Ni}_n\text{O}_{3n+1} \cdot \text{La}_{m+1}\text{Ni}_m\text{O}_{3m+1}$ ($n \neq m$). Structurally, $\text{La}_5\text{Ni}_3\text{O}_{11}$ consists of alternating perovskite-like layers of La_2NiO_4 ($n = 1$) and $\text{La}_3\text{Ni}_2\text{O}_7$ ($m = 2$) resulting in a 1-2-1-2 layering motif (see Fig. 1(a)). At ambient pressure, the crystal structure is orthorhombic with $Cmmm$ crystal symmetry, containing two inequivalent Ni sites: Ni1 in the bilayer and Ni2 in the single-layer block. As mentioned above, in contrast to the ‘conven-

tional’ bilayer nickelate $\text{La}_3\text{Ni}_2\text{O}_7$ (referred to as ‘2222’), the NiO_6 octahedra in $\text{La}_5\text{Ni}_3\text{O}_{11}$ at ambient pressure exhibit no tilts as both the in-plane and out-of-plane Ni-O-Ni bond angles are 180° . However, some structural ambiguities remain in the $\text{La}_5\text{Ni}_3\text{O}_{11-1212}$ compound as non-superconducting samples have also been resolved in the $Immm$ space group at ambient pressure [41]. Formal valence counting gives an average $\text{Ni}(3d)$ occupation of $d^{7.67}$. For the structural constituents $n = 1$ and $n = 2$ RPs, the average $\text{Ni}(3d)$ occupations are d^8 and $d^{7.5}$, respectively. Hence, in terms of $\text{Ni}(3d)$ occupation, the hybrid RP nickelate represents an average of its $n = 1$ and $n = 2$ structural constituents.

Figure 1(b) provides the non-magnetic DFT description of the band structure of $\text{La}_5\text{Ni}_3\text{O}_{11-1212}$ using the ‘fatspectral’ representation [63] to emphasize the $\text{Ni}(3d)$ orbital content. Bands of $\text{Ni}-e_g$ character (hybridized with $\text{O}(2p)$ states) from both the single-layer and bilayer blocks can be observed in the vicinity of the Fermi level (ε_F): two $\text{Ni}-d_{x^2-y^2}$ bands from the bilayer and one from the single-layer block (blue), as well as one d_{z^2} band from the single-layer and two $\text{Ni}-d_{z^2}$ from the bilayer (pink) – the latter forming a bonding (B)-antibonding (AB) combination due to quantum confinement [64–66]. The bonding $\text{Ni}-d_{z^2}$ sits just below ε_F , while the anti-bonding $\text{Ni}-d_{z^2}$ band is ~ 1 eV above ε_F . The $\text{Ni}-d_{z^2}$ band from the single-layer block sits in between the B-AB bands from the bilayer. The $\text{Ni}-t_{2g}$ bands span a 1 eV window between -2 and -1 eV relative to ε_F . The corresponding Fermi surface at the DFT level in the $k_z = 0$ plane is shown in Fig. 1(d) where four Fermi surface sheets can be observed. Two sheets come primarily from the bilayer Ni1 site: a circular electron-like pocket (α) and a hole-pocket of mixed $\text{Ni}-e_g/\text{Ni}-d_{x^2-y^2}$ character (β). The remaining two sheets are contributed by the single-layer Ni2 site: a large hole pocket around the M point with $\text{Ni}-d_{z^2}$ character (γ') and a square pocket at the zone center with $\text{Ni}-d_{x^2-y^2}$ character (α'). Thus, the electronic structure of $\text{La}_5\text{Ni}_3\text{O}_{11-1212}$ at the DFT level is quite different from that of the bilayer RP $\text{La}_3\text{Ni}_2\text{O}_7$ -2222 where only the α and β bands are present at the Fermi level [14, 66].

As shown in previous work [47, 48], a non-magnetic DFT description may not be sufficient to provide a faithful description of the electronic structure of the existing hybrid RP nickelates, as it cannot account for a Mott-insulating state in the single-layer La_2NiO_4 . This conclusion is particularly obvious in the single-layer trilayer polymorph of $\text{La}_3\text{Ni}_2\text{O}_7$ -1313. In this material, the electronic structure at the non-magnetic DFT level also shows extra Fermi surface sheets coming from the single-layer block [45, 48]. However, recent ARPES experiments do not show any evidence for these extra sheets [49]. The electronic structure observed in ARPES can instead be easily captured by including beyond DFT electronic correlations: in DFT+DMFT the single-layer block is indeed gapped (in line with the Mott insulating state of bulk La_2NiO_4 [67]), and the only contributions at the Fermi level become those from the trilayer block, in

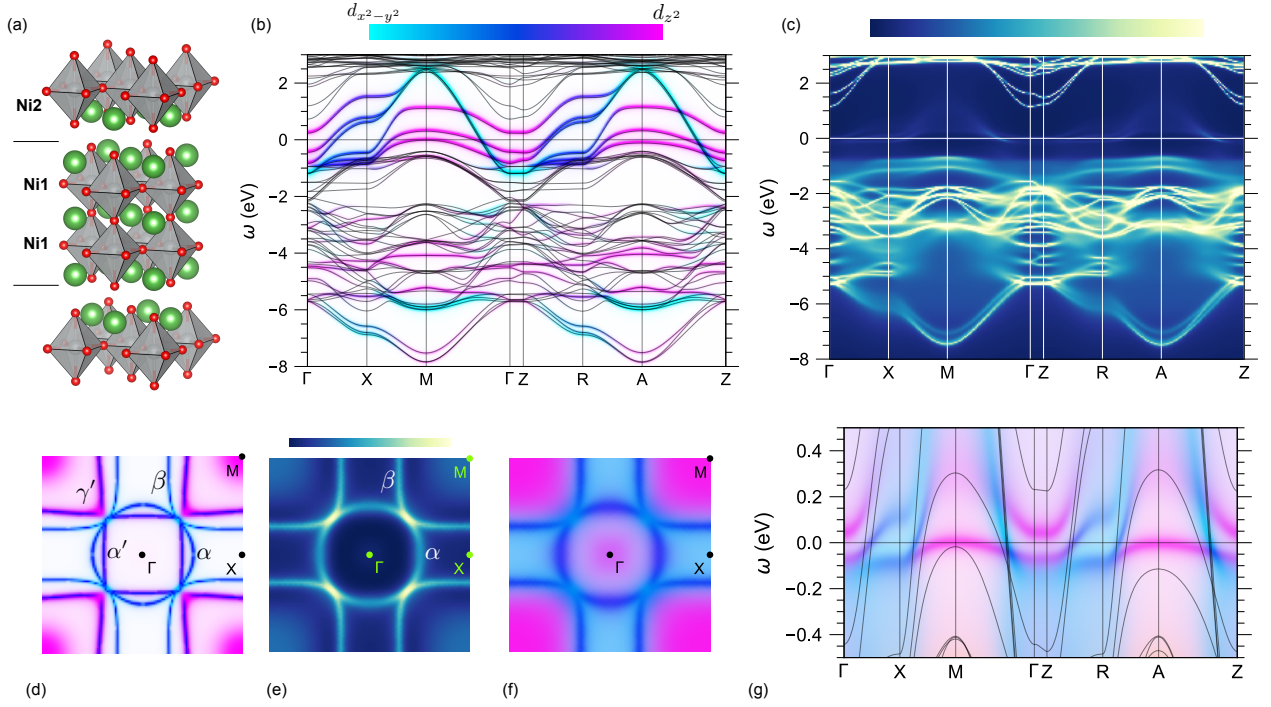


FIG. 1. Structure and \mathbf{k} -dependent data of $\text{La}_5\text{Ni}_3\text{O}_{11}$ at ambient pressure from DFT (b,d) and DFT+DMFT at $T \sim 150$ K (c,e-g). (a) Crystal structure of $\text{La}_5\text{Ni}_3\text{O}_{11}$ in the $Cmmm$ space group with inequivalent Ni sites denoted: Ni1 in the bilayer, and Ni2 in the single-layer block. (b) LDA band structure along high-symmetry lines in the Brillouin zone using the “fatspectral” representation of the Ni(3d) orbitals. (c) False-color plot of the spectral function in a large energy window along high symmetry directions in the Brillouin zone. (d) LDA Fermi surface in the $k_z = 0$ plane in the Ni(3d) “fatspectral” representation. (e,f) Interacting Fermi surfaces in the $k_z = 0$ plane: false-color plot (left) and Ni(3d)-projected (right). (g) Low-energy blow up of the interacting spectral function in (c) using the Ni(3d) fatspectral representation where thin lines denote the LDA band structure.

agreement with ARPES. With these considerations, we now turn to the role of local electronic correlations in $\text{La}_5\text{Ni}_3\text{O}_{11-1212}$ using DFT+DMFT.

Correlated electronic structure at ambient pressure.— Figure 1(c,g) shows the \mathbf{k} -resolved spectral data for $\text{La}_5\text{Ni}_3\text{O}_{11}$ at ambient pressure from DFT+DMFT at $T \sim 150$ K ($\beta = 1/T = 77$ eV $^{-1}$). The Ni- e_g dominated parts of the spectrum are very strongly correlated with large scattering rates for both Ni1 (bilayer) and Ni2 (single-layer), which results in heavily renormalized and decoherent Ni- e_g dispersions in both orbital sectors (see below). Importantly, the Ni2- d_{z^2} component of the self-energy is diverging (see Fig. 2(b)) indicating the opening of a Mott gap in the single-layer block. Similarly to the results in $\text{La}_3\text{Ni}_2\text{O}_7$ -1313 [47, 48], DFT+DMFT calculations in $\text{La}_5\text{Ni}_3\text{O}_{11-1212}$ reveal a much simpler electronic structure relative to that of DFT as only the bilayer contributes to the low-energy physics with two Ni1- $d_{x^2-y^2}$ bands (blue color) and the flat bonding Ni1- d_{z^2} (pink color) remaining around ε_F . The spectral weight corresponding to the anti-bonding Ni1- d_{z^2} is renormalized to +0.3 eV above ε_F , while the Ni- t_{2g} dispersions remain below the chemical potential. The interacting Fermi surface in Fig. 1(e,f) clearly reflects the simplified electronic structure obtained at the DFT+DMFT level

for $\text{La}_5\text{Ni}_3\text{O}_{11-1212}$. Only two Fermi surface sheets can now be observed: the circular electron pocket (α) and the large hole-like pocket (β), both with predominant Ni- $d_{x^2-y^2}$ orbital character. The effect of local dynamical correlations is to remove the Fermi surface sheets contributed by the single-layer block, leaving only the bilayer sheets. Thus, by incorporating electronic correlations, we find an emergent electronic structure in $\text{La}_5\text{Ni}_3\text{O}_{11-1212}$ that is nearly identical to that of $\text{La}_3\text{Ni}_2\text{O}_7$ -2222 at ambient pressure [49, 68], as obtained from ARPES experiments.

To further elucidate correlation effects on the electronic structure of $\text{La}_5\text{Ni}_3\text{O}_{11-1212}$, we analyze the site-resolved local Ni(3d) \mathbf{k} -integrated spectral functions and Matsubara Ni- e_g self-energies shown in Fig. 2(b). The local spectral function on the Ni1 site corresponding to the bilayer reveals a broad Ni- d_{z^2} and Ni- $d_{x^2-y^2}$ spectral weight, indicating decoherence in both orbital sectors, as mentioned above. The local spectral function on the Ni2 site corresponding to the single-layer exhibits a small Ni- $d_{x^2-y^2}$ peak at ε_F and a small amount of Ni- d_{z^2} spectral weight remains due to the diverging self-energy. The site-resolved Ni- e_g Matsubara self-energies are shown in the right panel of Fig. 2(b). From the low-Matsubara behavior of the self-energy, we can determine key fea-

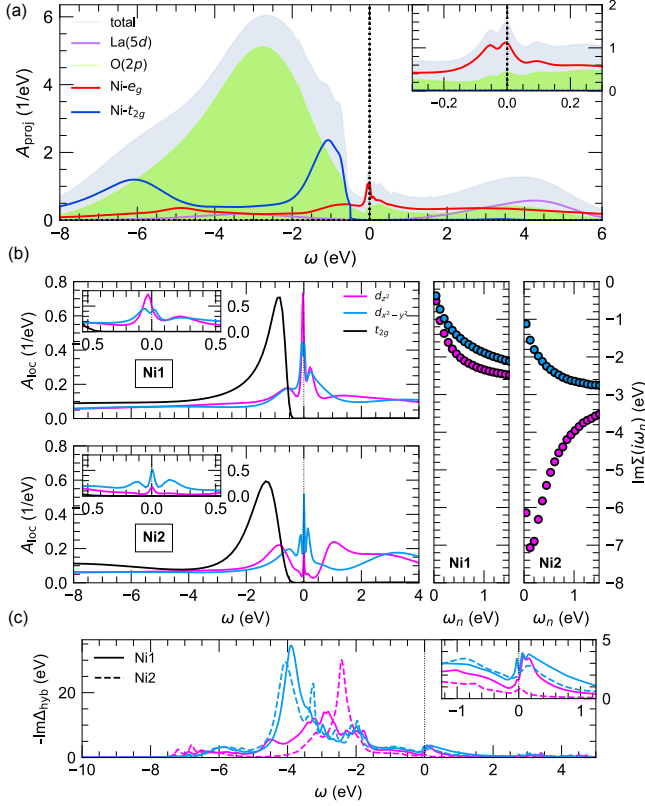


FIG. 2. Total- and site-resolved \mathbf{k} -integrated spectral data of $\text{La}_5\text{Ni}_3\text{O}_{11}$ at ambient pressure ($Cmmm$) at $T \sim 150$ K. (a) Orbital-projected spectral function (inset: low-energy blow up). (b) Left panel: site-resolved local $\text{Ni}(3d)$ spectral functions (inset: low-energy blow up). Right panel: site-resolved local $\text{Ni-}e_g$ imaginary part of the Matsubara self-energies. (c) Site-resolved $\text{Ni-}e_g$ hybridization functions (inset: low-energy blow up).

tures of the correlated electronic structure. As a metric for the strength of electronic correlations, the mass enhancement $m^*/m_{\text{DFT}} = 1 - \partial_{\omega_n} \text{Im}\Sigma(i\omega_n)|_{i\omega_n \rightarrow 0}$ is often used. Fitting a fourth order polynomial ($\text{Im}\Sigma(i\omega_n > 0) \approx \sum_p a_p \omega_n^p$) to the lowest six Matsubara frequencies yields $m_{d_{z^2}}^* \sim 10$ and $m_{d_{x^2-y^2}}^* \sim 8$ for the bilayer Ni (Ni1), which are comparable to bulk ambient pressure $\text{La}_3\text{Ni}_2\text{O}_7$ -2222 [16]. The scattering rate ($\propto -\text{Im}\Sigma(i\omega_n)|_{i\omega_n \rightarrow 0}$) on both $\text{Ni-}e_g$ orbitals remains large at this temperature underpinning the ‘washed out’ spectral features in the \mathbf{k} -dependent data rendering the bilayer in a bad metal or incoherent metallic state. The $\text{Ni2-}e_g$ self-energies are close to a Mott instability with a diverging $\text{Ni-}d_{z^2}$ component and large $\text{Ni-}d_{x^2-y^2}$ component.

To connect the local spectrum back to the Bloch spectrum, we analyze the DMFT hybridization function $\Delta_{\text{hyb}}(\omega) = \omega + \mu - G_{\text{loc}}^{-1}(\omega) - \Sigma_{\text{imp}}(\omega)$. The hybridization function $-\text{Im}\Delta_{\text{hyb}}$ shown in Fig. 2(c) reaffirms the distinct orbital- and site-selective behavior. For the Ni1 site, both orbitals exhibit large finite values of $\text{Im}\Delta(\omega = 0)$,

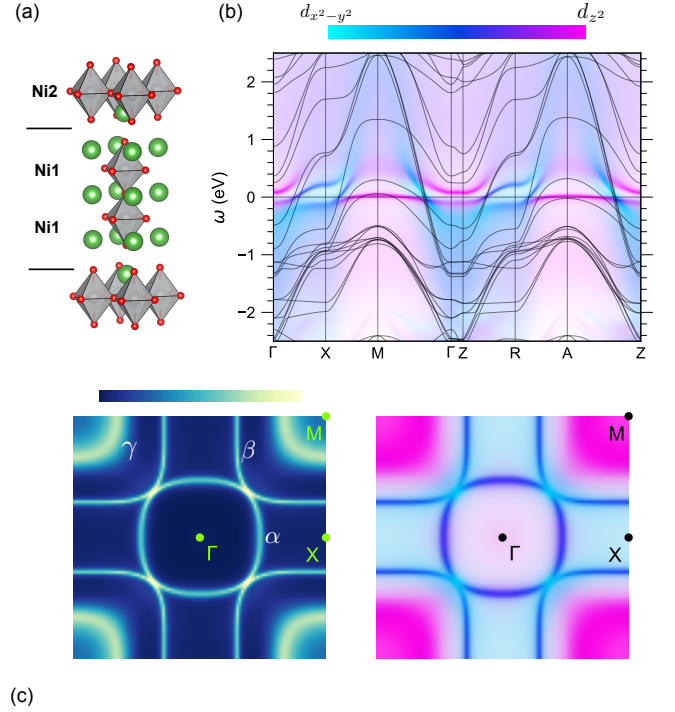


FIG. 3. \mathbf{k} -dependent spectral data of $\text{La}_5\text{Ni}_3\text{O}_{11}$ at 15 GPa ($P4/mmm$) from DFT+DMFT at $T \sim 116$ K. (a) Crystal structure of $\text{La}_5\text{Ni}_3\text{O}_{11}$ in the $P4/mmm$ space group with inequivalent Ni sites labeled. (b) Interacting spectral function in $\text{Ni}(3d)$ fatspectral representation along high-symmetry lines. Thin, black lines correspond to the LDA band structure. (c) Interacting Fermi surface in the $k_z = 0$ plane: false-color plot (left) and $\text{Ni}(3d)$ -projected (right).

indicative of strong hybridization with the bath and itinerant electrons. In contrast, the Ni2 site shows orbital differentiation (in line with the Ni2 self-energies): the $\text{Ni-}d_{z^2}$ orbital exhibits vanishing hybridization at low frequencies, signaling strong localization and effective decoupling from the bath, while the $\text{Ni-}d_{x^2-y^2}$ orbital retains a finite, though significantly reduced, hybridization, pointing to weak coupling to metallic states. Combining this analysis with the Matsubara self-energies, the data support a picture of orbital- and site-selective localization, where Ni2 hosts a Mott-localized orbital and a weakly hybridized, incoherent metallic orbital, while Ni1 exhibits itinerancy without coherence.

To scrutinize orbital admixture effects on the electronic structure of $\text{La}_5\text{Ni}_3\text{O}_{11}$ -1212 at ambient pressure, we carefully examine the total and orbital-projected \mathbf{k} -integrated spectral data including the $\text{O}(2p)$ states (see Fig. 2(a)). The sizeable admixture of $\text{Ni-}e_g$ and $\text{O}(2p)$ content can be observed. Furthermore, the spectral features include broad $\text{O}(2p)$ peak at -3.5 eV and a $\text{Ni}(3d)$ peak -0.5 eV. The dominant d and p peaks can be translated into a charge-transfer energy $\Delta_{\text{CT}} = \varepsilon_d - \varepsilon_p \sim 3$ eV. We observe only minor $\text{La}(5d)$ weight located within the broader $\text{O}(2p)$ peak. Total $\text{Ni}(3d)$ occupations read ~ 8.2

for both Ni sites indicating sizeable hole character on the oxygens [16, 47, 69]. Ultimately, in terms of filling, both Ni sites exhibit nearly half-filled Ni- e_g orbitals [16, 70]. To summarize, the DFT+DMFT electronic structure of $\text{La}_5\text{Ni}_3\text{O}_{11-1212}$ at ambient pressure is very similar to that of $\text{La}_3\text{Ni}_2\text{O}_7$ -2222 as shown in the spectral data. We subsequently analyze the evolution of the electronic structure of the single-layer bilayer RP nickelate under pressure.

Correlated electronic structure at 15 GPa.— $\text{La}_5\text{Ni}_3\text{O}_{11-1212}$ becomes superconducting when moderate pressures are applied (~ 10 -25 GPa) [44]. The emergence of superconductivity is concomitant with the suppression of a density-wave-like state and a structural transition from an orthorhombic to a tetragonal space group symmetry (see Fig. 3(a)) [44], akin to its bilayer counterpart [71–76]. The momentum-resolved spectral function for $\text{La}_5\text{Ni}_3\text{O}_{11}$ at 15 GPa from DFT+DMFT at $T \sim 116$ K is shown in Fig. 3(b) within the fatspectral representation. Increased electronic bandwidths can be observed as a consequence of the the reduction in lattice constants (of $\sim 2\%$) and the related contraction of NiO_6 octahedra. The combination of pressure and lower temperature increase the coherence giving rise to quasiparticle (QP) dispersions. The key low-energy dispersions are once again of Ni- e_g orbital content stemming exclusively from the bilayer. The most relevant effect of pressure is the pinning of the bonding Ni- d_{z^2} dispersion at ε_F . As a consequence, the interacting Fermi surface (shown in Fig. 3(c)) now shows a third pocket of d_{z^2} character at the zone corners (γ) – in addition to the α and β sheets obtained at ambient pressure. While studying the superconducting pairing symmetry of $\text{La}_5\text{Ni}_3\text{O}_{11-1212}$ would require a tailored model Hamiltonian study (which is beyond the scope of this work), we note that the appearance of the γ corner pocket in bulk $\text{La}_3\text{Ni}_2\text{O}_7$ under pressure has been linked to the emergence of superconductivity [19, 22–26, 33].

The \mathbf{k} -integrated spectral data and site-resolved local quantities are summarized in Fig. 4. The total- and orbital-resolved spectral function in Fig. 4(a) reveals broad O($2p$) and Ni($3d$) peaks at ~ -4 eV and -0.75 eV, respectively, resulting in a slightly increased charge-transfer energy relative to ambient pressure [66]. The metallic spectral weight is dominantly Ni- e_g in character with some admixture of O($2p$) content. A sharp peak at ε_F has emerged due to the increased coherence. There is no contribution from the Ni- t_{2g} orbitals around ε_F . The effect of pressure on the local Ni sites is subtle (see Fig. 4(b)). As pressure increases the electronic bandwidth, electronic correlations are weakened for both Ni sites, as evidenced by the self-energies in Fig. 4(b), where the reduced mass enhancements are $m_{z^2} \sim 7$ and $m_{x^2-y^2} \sim 2$. In addition to the reduced mass enhancements, the scattering rates have also decreased consistent with the increased coherence of both orbitals in the bilayer. Connecting the total spectrum to the local spectrum, we find that the sharp QP-like peak in the total spectrum

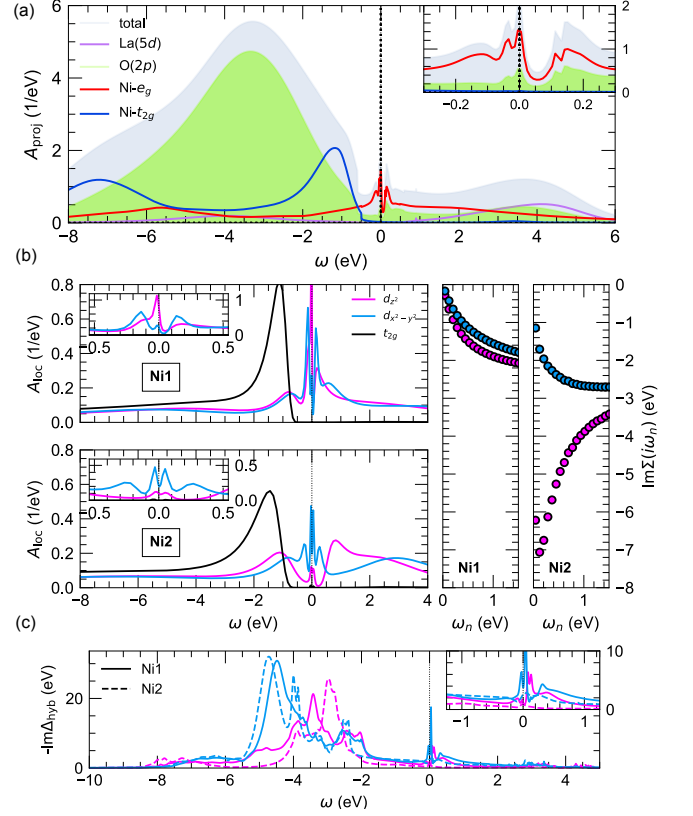


FIG. 4. Total- and site-resolved \mathbf{k} -integrated spectral data of $\text{La}_5\text{Ni}_3\text{O}_{11}$ at 15 GPa ($P4/mmm$) at $T \sim 116$ K. (a) Orbital-projected spectral function (inset: low-energy blow up). (b) Left panel: site-resolved local Ni($3d$) spectral functions (inset: low-energy blow up). Right panel: site-resolved local Ni- e_g imaginary part of the Matsubara self-energies. (c) Site-resolved Ni- e_g hybridization functions (inset: low-energy blow up).

can be assigned to the Ni- d_{z^2} orbital within the bilayer associated with the flat-band in the \mathbf{k} -resolved spectral function (see Fig. 3(b)). This coincides with the reduced $\text{Im}\Delta_{\text{hyb}}$ for Ni1- d_{z^2} (See Fig. 4(c)). Additionally, the effect of pressure has transformed the broad Ni- $d_{x^2-y^2}$ spectral weight at ambient pressure into a subtle QP-like peak with large hybridization function at ε_F denoting itinerant character. We emphasize the two key features of the pressurized electronic structure of $\text{La}_5\text{Ni}_3\text{O}_{11}$: the absence of contributions from the single-layer block to the low-energy electronic structure, and the emergence of the γ pocket at the zone corners, which is consistent with pressurized $\text{La}_3\text{Ni}_2\text{O}_7$ -2222.

IV. SUMMARY AND DISCUSSION

By combining density-functional theory and dynamical mean-field theory, we have identified several relevant features in the electronic structure of the single-layer bilayer hybrid RP nickelate $\text{La}_5\text{Ni}_3\text{O}_{11}$ at both ambient and high

pressure. Incorporating electronic correlations reveals layer-selective behavior in $\text{La}_5\text{Ni}_3\text{O}_{11}$, as the single-layer is effectively localized – either in or near a Mott insulating state – while the bilayer remains metallic but strongly correlated. Thus, our results suggest that the low-energy physics of this hybrid RP nickelate is dominated by the bilayer block while the single-layer acts primarily as a ‘spectator’ and is unlikely to drive the observed superconductivity. As a consequence, the electronic structure of $\text{La}_5\text{Ni}_3\text{O}_{11-1212}$ is very similar to that of the bilayer RP $\text{La}_3\text{Ni}_2\text{O}_7-2222$, suggesting that they are susceptible to the same low-energy phenomena. In both materials two Fermi surface sheets are present at ambient pressure (α and β) of dominant $d_{x^2-y^2}$ character. Under pressure, an extra corner pocket γ of pure d_{z^2} character arises that has been linked to the emergence of superconductivity in the bilayer RP. Within the metallic bilayer, orbital-selective differentiation emerges: the flat Ni- d_{z^2} orbitals show strong correlations and a high density of states, while the Ni- $d_{x^2-y^2}$ are also correlated but more itinerant. The striking similarities in the electronic structure of $\text{La}_3\text{Ni}_2\text{O}_7-2222$ and $\text{La}_5\text{Ni}_3\text{O}_{11-1212}$ (despite obvious differences in the structure and electron count) suggest

an important role of the bilayer structural motif and universal features in the electronic structure necessary for superconductivity to arise in RP nickelates.

Future interesting directions include ARPES and optical spectroscopy as probes of the electronic structure of $\text{La}_5\text{Ni}_3\text{O}_{11-1212}$ at ambient pressure and tests of the theory presented here. Given the exciting developments in the thin-film community on strained $\text{La}_3\text{Ni}_2\text{O}_7$ [77] and variants [78] we envision that strain-induced superconductivity in this hybrid RP will also be an interesting avenue to explore both experimentally and theoretically. Furthermore, it will be promising to span the studies of correlated phenomena in higher-order (n, m) hybrid RP nickelates.

ACKNOWLEDGMENTS

The Flatiron Institute is a division of the Simons Foundation. ASB was supported by NSF grant No. DMR-2045826.

-
- [1] H. Sun, M. Huo, X. Hu, J. Li, Z. Liu, Y. Han, L. Tang, Z. Mao, P. Yang, B. Wang, J. Cheng, D.-X. Yao, G.-M. Zhang, and M. Wang, Signatures of superconductivity near 80 K in a nickelate under high pressure, *Nature* **621**, 493 (2023).
 - [2] N. Wang, G. Wang, X. Shen, J. Hou, J. Luo, X. Ma, H. Yang, L. Shi, J. Dou, J. Feng, *et al.*, Bulk high-temperature superconductivity in pressurized tetragonal $\text{La}_2\text{PrNi}_2\text{O}_7$, *Nature* **634**, 579 (2024).
 - [3] J. Hou, P.-T. Yang, Z.-Y. Liu, J.-Y. Li, P.-F. Shan, L. Ma, G. Wang, N.-N. Wang, H.-Z. Guo, J.-P. Sun, Y. Uwatoko, M. Wang, G.-M. Zhang, B.-S. Wang, and J.-G. Cheng, Emergence of high-temperature superconducting phase in pressurized $\text{La}_3\text{Ni}_2\text{O}_7$ crystals, *Chin. Phys. Lett.* **40**, 117302 (2023).
 - [4] M. Zlang, C. Pei, D. Peng, X. Du, W. Hu, Y. Cao, Q. Wang, J. Wu, Y. Li, H. Liu, C. Wen, J. Song, Y. Zhao, C. Li, W. Cao, S. Zhu, Q. Zhang, N. Yu, P. Cheng, L. Zhang, Z. Li, J. Zhao, Y. Chen, C. Jin, H. Guo, C. Wu, F. Yang, Q. Zeng, S. Yan, L. Yang, and Y. Qi, Superconductivity in trilayer nickelate $\text{La}_4\text{Ni}_3\text{O}_{10}$ under pressure, *Phys. Rev. X* **15**, 021005 (2025).
 - [5] Q. Li, Y.-J. Zhang, Z.-N. Xiang, Y. Zhang, X. Zhu, and H.-H. Wen, Signature of superconductivity in pressurized $\text{La}_4\text{Ni}_3\text{O}_{10}$, *Chin. Phys. Lett.* **41**, 017401 (2024).
 - [6] Y. Zhu, D. Peng, E. Zhang, B. Pan, X. Chen, L. Chen, H. Ren, F. Liu, Y. Hao, N. Li, Z. Xing, F. Lan, J. Han, J. Wang, D. Jia, H. Wo, Y. Gu, Y. Gu, L. Ji, W. Wang, H. Gou, Y. Shen, T. Ying, X. Chen, W. Yang, H. Cao, C. Zheng, Q. Zeng, J.-g. Guo, and J. Zhao, Superconductivity in pressurized trilayer $\text{La}_4\text{Ni}_3\text{O}_{10-\delta}$ single crystals, *Nature* **631**, 531 (2024).
 - [7] D. Li, K. Lee, B. Y. Wang, M. Osada, S. Crossley, H. R. Lee, Y. Cui, Y. Hikita, and H. Y. Hwang, Superconductivity in an infinite-layer nickelate, *Nature* **572**, 624 (2019).
 - [8] M. Osada, B. Y. Wang, B. H. Goodge, K. Lee, H. Yoon, K. Sakuma, D. Li, M. Miura, L. F. Kourkoutis, and H. Y. Hwang, A superconducting praseodymium nickelate with infinite layer structure, *Nano Letters* **20**, 5735 (2020).
 - [9] M. Osada, B. Y. Wang, B. H. Goodge, S. P. Harvey, K. Lee, D. Li, L. F. Kourkoutis, and H. Y. Hwang, Nickelate superconductivity without rare-earth magnetism: $(\text{La}, \text{Sr})\text{NiO}_2$, *Adv. Mater.* **33**, 2104083 (2021).
 - [10] S. Zeng, C. Li, L. E. Chow, Y. Cao, Z. Zhang, C. S. Tang, X. Yin, Z. S. Lim, J. Hu, P. Yang, and A. Ariando, Superconductivity in infinite-layer nickelate $\text{La}_{1-x}\text{Ca}_x\text{NiO}_2$ thin films, *Sci Adv* **8**, eabl9927 (2022).
 - [11] G. A. Pan, D. Ferenc Segedin, H. LaBollita, Q. Song, E. M. Nica, B. H. Goodge, A. T. Pierce, S. Doyle, S. Novakov, D. Córdova Carrizales, A. T. N’Diaye, P. Shafer, H. Paik, J. T. Heron, J. A. Mason, A. Yacoby, L. F. Kourkoutis, O. Erten, C. M. Brooks, A. S. Botana, and J. A. Mundy, Superconductivity in a quintuple-layer square-planar nickelate, *Nat. Mater.* **21**, 160 (2022).
 - [12] L. Wang, Y. Li, S.-Y. Xie, F. Liu, H. Sun, C. Huang, Y. Gao, T. Nakagawa, B. Fu, B. Dong, Z. Cao, R. Yu, S. I. Kawaguchi, H. Kadobayashi, M. Wang, C. Jin, H.-k. Mao, and H. Liu, Structure responsible for the superconducting state in $\text{La}_3\text{Ni}_2\text{O}_7$ at high-pressure and low-temperature conditions, *J. Am. Chem. Soc.* **146**, 7506 (2024).
 - [13] M. Greenblatt, Ruddlesden-popper $\text{Ln}_{n+1}\text{Ni}_n\text{O}_{3n+1}$ nickelates: structure and properties, *Curr. Opin. Solid State Mater. Sci.* **2**, 174 (1997).
 - [14] Y. Zhang, L.-F. Lin, A. Moreo, and E. Dagotto, Electronic structure, dimer physics, orbital-selective behavior, and magnetic tendencies in the bilayer nickelate su-

- perconductor $\text{La}_3\text{Ni}_2\text{O}_7$ under pressure, *Phys. Rev. B* **108**, L180510 (2023).
- [15] X. Chen, P. Jiang, J. Li, Z. Zhong, and Y. Lu, Charge and spin instabilities in superconducting $\text{La}_3\text{Ni}_2\text{O}_7$, *Phys. Rev. B* **111**, 014515 (2025).
- [16] F. Lechermann, J. Gondolf, S. Bötzel, and I. M. Eremin, Electronic correlations and superconducting instability in $\text{La}_3\text{Ni}_2\text{O}_7$ under high pressure, *Phys. Rev. B* **108**, L201121 (2023).
- [17] V. Christiansson, F. Petocchi, and P. Werner, Correlated electronic structure of $\text{La}_3\text{Ni}_2\text{O}_7$ under pressure, *Phys. Rev. Lett.* **131**, 206501 (2023).
- [18] Z. Luo, X. Hu, M. Wang, W. Wú, and D.-X. Yao, Bilayer two-orbital model of $\text{La}_3\text{Ni}_2\text{O}_7$ under pressure, *Phys. Rev. Lett.* **131**, 126001 (2023).
- [19] Y. Gu, C. Le, Z. Yang, X. Wu, and J. Hu, Effective model and pairing tendency in bilayer Ni-based superconductor $\text{La}_3\text{Ni}_2\text{O}_7$, *arXiv:2306.07275* (2023).
- [20] Y. Shen, M. Qin, and G.-M. Zhang, Effective bilayer model hamiltonian and density-matrix renormalization group study for the high- T_c superconductivity in $\text{La}_3\text{Ni}_2\text{O}_7$ under high pressure, *Chin. Phys. Lett.* **40**, 127401 (2023).
- [21] W. Wú, Z. Luo, D.-X. Yao, and M. Wang, Charge transfer and zhang-rice singlet bands in the nickelate superconductor $\text{La}_3\text{Ni}_2\text{O}_7$ under pressure, *arXiv:2307.05662* (2023).
- [22] Q.-G. Yang, D. Wang, and Q.-H. Wang, Possible s_{\pm} -wave superconductivity in $\text{La}_3\text{Ni}_2\text{O}_7$, *Phys. Rev. B* **108**, L140505 (2023).
- [23] Y.-B. Liu, J.-W. Mei, F. Ye, W.-Q. Chen, and F. Yang, s^{\pm} -wave pairing and the destructive role of apical-oxygen deficiencies in $\text{La}_3\text{Ni}_2\text{O}_7$ under pressure, *Phys. Rev. Lett.* **131**, 236002 (2023).
- [24] Y. Zhang, L.-F. Lin, A. Moreo, T. A. Maier, and E. Dagotto, Structural phase transition, s_{\pm} -wave pairing, and magnetic stripe order in bilayered superconductor $\text{La}_3\text{Ni}_2\text{O}_7$ under pressure, *Nat. Commun* **15**, 2470 (2024).
- [25] X.-Z. Qu, D.-W. Qu, J. Chen, C. Wu, F. Yang, W. Li, and G. Su, Bilayer $t-J-J_{\perp}$ model and magnetically mediated pairing in the pressurized nickelate $\text{La}_3\text{Ni}_2\text{O}_7$, *Phys. Rev. Lett.* **132**, 036502 (2024).
- [26] Y.-F. Yang, G.-M. Zhang, and F.-C. Zhang, Interlayer valence bonds and two-component theory for high- T_c superconductivity of $\text{La}_3\text{Ni}_2\text{O}_7$ under pressure, *Phys. Rev. B* **108**, L201108 (2023).
- [27] Y. Zhang, L.-F. Lin, A. Moreo, T. A. Maier, and E. Dagotto, Trends in electronic structures and s_{\pm} -wave pairing for the rare-earth series in bilayer nickelate superconductor $\text{R}_3\text{Ni}_2\text{O}_7$, *Phys. Rev. B* **108**, 165141 (2023).
- [28] D.-C. Lu, M. Li, Z.-Y. Zeng, W. Hou, J. Wang, F. Yang, and Y.-Z. You, Superconductivity from doping symmetric mass generation insulators: Application to $\text{La}_3\text{Ni}_2\text{O}_7$ under pressure, *arXiv:2308.11195* (2023).
- [29] Y.-H. Tian, Y. Chen, J.-M. Wang, R.-Q. He, and Z.-Y. Lu, Correlation effects and concomitant two-orbital s_{\pm} -wave superconductivity in $\text{La}_3\text{Ni}_2\text{O}_7$ under high pressure, *Phys. Rev. B* **109**, 165154 (2024).
- [30] J. Huang, Z. D. Wang, and T. Zhou, Impurity and vortex states in the bilayer high-temperature superconductor $\text{La}_3\text{Ni}_2\text{O}_7$, *Phys. Rev. B* **108**, 174501 (2023).
- [31] R. Jiang, J. Hou, Z. Fan, Z.-J. Lang, and W. Ku, Pressure driven fractionalization of ionic spins results in cuprate-like high- T_c superconductivity in $\text{La}_3\text{Ni}_2\text{O}_7$, *Phys. Rev. Lett.* **132**, 126503 (2024).
- [32] Z. Liao, L. Chen, G. Duan, Y. Wang, C. Liu, R. Yu, and Q. Si, Electron correlations and superconductivity in $\text{La}_3\text{Ni}_2\text{O}_7$ under pressure tuning, *Phys. Rev. B* **108**, 214522 (2023).
- [33] C. Lu, Z. Pan, F. Yang, and C. Wu, Interlayer-coupling-driven high-temperature superconductivity in $\text{La}_3\text{Ni}_2\text{O}_7$ under pressure, *Phys. Rev. Lett.* **132**, 146002 (2024).
- [34] H. Oh and Y.-H. Zhang, Type-II $t-J$ model and shared superexchange coupling from Hund's rule in superconducting $\text{La}_3\text{Ni}_2\text{O}_7$, *Phys. Rev. B* **108**, 174511 (2023).
- [35] Q. Qin and Y.-f. Yang, High- T_c superconductivity by mobilizing local spin singlets and possible route to higher T_c in pressurized $\text{La}_3\text{Ni}_2\text{O}_7$, *Phys. Rev. B* **108**, L140504 (2023).
- [36] H. Sakakibara, N. Kitamine, M. Ochi, and K. Kuroki, Possible high T_c superconductivity in $\text{La}_3\text{Ni}_2\text{O}_7$ under high pressure through manifestation of a nearly half-filled bilayer Hubbard model, *Phys. Rev. Lett.* **132**, 106002 (2024).
- [37] D. A. Shilenko and I. V. Leonov, Correlated electronic structure, orbital-selective behavior, and magnetic correlations in double-layer $\text{La}_3\text{Ni}_2\text{O}_7$ under pressure, *Phys. Rev. B* **108**, 125105 (2023).
- [38] H. Sakakibara, M. Ochi, H. Nagata, Y. Ueki, H. Sakurai, R. Matsumoto, K. Terashima, K. Hirose, H. Ohta, M. Kato, Y. Takano, and K. Kuroki, Theoretical analysis on the possibility of superconductivity in the trilayer ruddlesden-popper nickelate $\text{La}_4\text{Ni}_3\text{O}_{10}$ under pressure and its experimental examination: Comparison with $\text{La}_3\text{Ni}_2\text{O}_7$, *Phys. Rev. B* **109**, 144511 (2024).
- [39] X.-W. Yi, Y. Meng, J.-W. Li, Z.-W. Liao, W. Li, J.-Y. You, B. Gu, and G. Su, Nature of charge density waves and metal-insulator transition in pressurized $\text{La}_3\text{Ni}_2\text{O}_7$, *Phys. Rev. B* **110**, L140508 (2024).
- [40] H. LaBollita, V. Pardo, M. R. Norman, and A. S. Botana, Assessing spin-density wave formation in $\text{La}_3\text{Ni}_2\text{O}_7$ from electronic structure calculations, *Phys. Rev. Mater.* **8**, L111801 (2024).
- [41] F. Li, N. Guo, Q. Zheng, Y. Shen, S. Wang, Q. Cui, C. Liu, S. Wang, X. Tao, G.-M. Zhang, and J. Zhang, Design and synthesis of three-dimensional hybrid Ruddlesden-Popper nickelate single crystals, *Phys. Rev. Mater.* **8**, 053401 (2024).
- [42] P. Puphal, P. Reiss, N. Enderlein, Y.-M. Wu, G. Khalullin, V. Sundaramurthy, T. Priessnitz, M. Knauff, A. Suthar, L. Richter, M. Isobe, P. A. van Aken, H. Takagi, B. Keimer, Y. E. Suyolcu, B. Wehinger, P. Hansmann, and M. Hepting, Unconventional crystal structure of the high-pressure superconductor $\text{La}_3\text{Ni}_2\text{O}_7$, *Phys. Rev. Lett.* **133**, 146002 (2024).
- [43] S. N. Abadi, K.-J. Xu, E. G. Lomeli, P. Puphal, M. Isobe, Y. Zhong, A. V. Fedorov, S.-K. Mo, M. Hashimoto, D.-H. Lu, B. Moritz, B. Keimer, T. P. Devereaux, M. Hepting, and Z.-X. Shen, Electronic structure of the alternating monolayer-trilayer phase of $\text{La}_3\text{Ni}_2\text{O}_7$, *arXiv:2402.07143* (2024).
- [44] M. Shi, D. Peng, K. Fan, Z. Xing, S. Yang, Y. Wang, H. Lin, R. Wu, M. Du, B. Ge, Z. Zeng, Q. Zeng, J. Ying, T. Wu, and X. Chen, Superconductivity of the hybrid Ruddlesden-Popper $\text{La}_5\text{Ni}_3\text{O}_{11}$ single crystals under high pressure, *arXiv:2502.01018* (2025).

- [45] X. Chen, J. Zhang, A. S. Thind, S. Sharma, H. LaBollita, G. Peterson, H. Zheng, D. P. Phelan, A. S. Botana, R. F. Klie, and J. F. Mitchell, Polymorphism in the Ruddlesden–Popper nickelate $\text{La}_3\text{Ni}_2\text{O}_7$: Discovery of a hidden phase with distinctive layer stacking, *J. Am. Chem. Soc.* **146**, 3640 (2024).
- [46] H. Wang, L. Chen, A. Rutherford, H. Zhou, and W. Xie, Long-range structural order in a hidden phase of Ruddlesden–Popper bilayer nickelate $\text{La}_3\text{Ni}_2\text{O}_7$, *Inorg. Chem.* **63**, 5020 (2024).
- [47] F. Lechermann, S. Bötzel, and I. M. Eremin, Electronic instability, layer selectivity, and fermi arcs in $\text{La}_3\text{Ni}_2\text{O}_7$, *Phys. Rev. Mater.* **8**, 074802 (2024).
- [48] H. LaBollita, S. Bag, J. Kapeghian, and A. S. Botana, Electronic correlations, layer distinction, and electron doping in the alternating single-layer–trilayer $\text{La}_3\text{Ni}_2\text{O}_7$ polymorph, *Phys. Rev. B* **110**, 155145 (2024).
- [49] C. C. Au-Yeung, X. Chen, S. Smit, M. Bluschke, V. Zimmermann, M. Michiardi, P. Moen, J. Kraan, C. S. B. Pang, C. T. Suen, S. Zhdanovich, M. Zonno, S. Gorovikov, Y. Liu, G. Levy, I. S. Elfimov, M. Berciu, G. A. Sawatzky, J. F. Mitchell, and A. Damascelli, Universal electronic structure of layered nickelates via oxygen-centered planar orbitals, [arXiv:2502.20450](https://arxiv.org/abs/2502.20450) (2025).
- [50] Y. Zhang, L.-F. Lin, A. Moreo, T. A. Maier, and E. Dagotto, Electronic structure, self-doping, and superconducting instability in the alternating single-layer trilayer stacking nickelates $\text{La}_3\text{Ni}_2\text{O}_7$, *Phys. Rev. B* **110**, L060510 (2024).
- [51] Y. Zhang, L.-F. Lin, A. Moreo, S. Okamoto, T. A. Maier, and E. Dagotto, Electronic structure, magnetic and pairing tendencies of alternating single-layer bilayer stacking nickelate $\text{La}_5\text{Ni}_3\text{O}_{11}$ under pressure, [arXiv:2503.05075](https://arxiv.org/abs/2503.05075) (2025).
- [52] P. Blaha, K. Schwarz, F. Tran, R. Laskowski, G. K. H. Madsen, and L. D. Marks, WIEN2k: An APW+lo program for calculating the properties of solids, *J. Chem. Phys.* **152**, 074101 (2020).
- [53] M. Aichhorn, L. Pourovskii, P. Seth, V. Vildosola, M. Zingl, O. E. Peil, X. Deng, J. Mravlje, G. J. Kraberger, C. Martins, M. Ferrero, and O. Parcollet, TRIQS/DFTTools: A TRIQS application for ab initio calculations of correlated materials, *Comput. Phys. Commun.* **204**, 200 (2016).
- [54] M. Aichhorn, L. Pourovskii, V. Vildosola, M. Ferrero, O. Parcollet, T. Miyake, A. Georges, and S. Biermann, Dynamical mean-field theory within an augmented plane-wave framework: Assessing electronic correlations in the iron pnictide LaFeAsO , *Phys. Rev. B* **80**, 085101 (2009).
- [55] P. Seth, I. Krivenko, M. Ferrero, and O. Parcollet, TRIQS/CTHYB: A continuous-time quantum Monte Carlo hybridisation expansion solver for quantum impurity problems, *Comput. Phys. Commun.* **200**, 274 (2016).
- [56] O. Parcollet, M. Ferrero, T. Ayral, H. Hafermann, I. Krivenko, L. Messio, and P. Seth, TRIQS: A toolbox for research on interacting quantum systems, *Comput. Phys. Commun.* **196**, 398 (2015).
- [57] M. T. Czyżyk and G. A. Sawatzky, Local-density functional and on-site correlations: The electronic structure of La_2CuO_4 and LaCuO_3 , *Phys. Rev. B* **49**, 14211 (1994).
- [58] G. J. Kraberger, R. Triebl, M. Zingl, and M. Aichhorn, Maximum entropy formalism for the analytic continuation of matrix-valued Green’s functions, *Phys. Rev. B* **96**, 155128 (2017).
- [59] G. Kresse and J. Hafner, Ab initio molecular dynamics for liquid metals, *Phys. Rev. B* **47**, 558 (1993).
- [60] G. Kresse and J. Furthmüller, Efficient iterative schemes for ab initio total-energy calculations using a plane-wave basis set, *Phys. Rev. B* **54**, 11169 (1996).
- [61] G. Kresse and D. Joubert, From ultrasoft pseudopotentials to the projector augmented-wave method, *Phys. Rev. B* **59**, 1758 (1999).
- [62] For structural relaxations, the plane-wave cut off was set to 600 eV and the force convergence criterion was set to 1 meV/Å. Integration in the Brillouin zone was done a $7 \times 7 \times 2$ k -grid with a 0.01 eV Gaussian smearing.
- [63] F. Lechermann, Emergent flat-band physics in $d^{9-\delta}$ multilayer nickelates, *Phys. Rev. B* **105**, 155109 (2022).
- [64] V. Pardo and W. E. Pickett, Quantum confinement induced molecular correlated insulating state in $\text{La}_4\text{Ni}_3\text{O}_8$, *Phys. Rev. Lett.* **105**, 266402 (2010).
- [65] M.-C. Jung, J. Kapeghian, C. Hanson, B. Pamuk, and A. S. Botana, Electronic structure of higher-order Ruddlesden–Popper nickelates, *Phys. Rev. B* **105**, 085150 (2022).
- [66] H. LaBollita, V. Pardo, M. R. Norman, and A. S. Botana, Electronic structure and magnetic properties of $\text{La}_3\text{Ni}_2\text{O}_7$ under pressure, [arXiv:2309.17279](https://arxiv.org/abs/2309.17279) (2023).
- [67] R. J. Cava, B. Batlogg, T. T. Palstra, J. J. Krajewski, W. F. Peck, A. P. Ramirez, and L. W. Rupp, Magnetic and electrical properties of $\text{La}_{2-x}\text{SrNiO}_{4\pm\delta}$, *Phys. Rev. B* **43**, 1229 (1991).
- [68] J. Yang, H. Sun, X. Hu, Y. Xie, T. Miao, H. Luo, H. Chen, B. Liang, W. Zhu, G. Qu, C.-Q. Chen, M. Huo, Y. Huang, S. Zhang, F. Zhang, F. Yang, Z. Wang, Q. Peng, H. Mao, G. Liu, Z. Xu, T. Qian, D.-X. Yao, M. Wang, L. Zhao, and X. J. Zhou, Orbital-dependent electron correlation in double-layer nickelate $\text{La}_3\text{Ni}_2\text{O}_7$, *Nat. Commun.* **15**, 4373 (2024).
- [69] F. Lechermann, Assessing the correlated electronic structure of lanthanum nickelates, *Electron. Struct.* **4**, 015005 (2022).
- [70] D. A. Shilenko and I. V. Leonov, Correlated electronic structure, orbital-selective behavior, and magnetic correlations in double-layer $\text{La}_3\text{Ni}_2\text{O}_7$ under pressure, *Phys. Rev. B* **108**, 125105 (2023).
- [71] Z. Liu, H. Sun, M. Huo, X. Ma, Y. Ji, E. Yi, L. Li, H. Liu, J. Yu, Z. Zhang, Z. Chen, F. Liang, H. Dong, H. Guo, D. Zhong, B. Shen, S. Li, and M. Wang, Evidence for charge and spin density waves in single crystals of $\text{La}_3\text{Ni}_2\text{O}_6$ and $\text{La}_3\text{Ni}_2\text{O}_7$, *Sci China Phys Mech Astron* **66**, 217411 (2023).
- [72] K. Chen, X. Liu, J. Jiao, M. Zou, Y. Luo, Q. Wu, N. Zhang, Y. Guo, and L. Shu, Evidence of spin density waves in $\text{La}_3\text{Ni}_2\text{O}_{7-\delta}$, [arXiv:2311.15717](https://arxiv.org/abs/2311.15717) (2023).
- [73] R. Khasanov, T. J. Hicken, D. J. Gawryluk, V. Sazgari, I. Plokhikh, L. P. Sorel, M. Bartkowiak, S. Bötzel, F. Lechermann, I. M. Eremin, H. Luetkens, and F. Guguchia, Pressure-enhanced splitting of density wave transitions in $\text{La}_3\text{Ni}_2\text{O}_{7-\delta}$, *Nat. Phys.* **21**, 430 (2025).
- [74] M. Kakoi, T. Oi, Y. Ohshita, M. Yashima, K. Kuroki, T. Kato, H. Takahashi, S. Ishiwata, Y. Adachi, N. Hatada, T. Uda, and H. Mukuda, Multiband metallic ground state in multilayered nickelates $\text{La}_3\text{Ni}_2\text{O}_7$ and $\text{La}_4\text{Ni}_3\text{O}_{10}$ probed by ^{139}La -NMR at ambient pressure, *J. Phys. Soc. Jpn* **93**, 053702 (2024).

- [75] X. Chen, J. Choi, Z. Jiang, J. Mei, K. Jiang, J. Li, S. Agrestini, M. Garcia-Fernandez, X. Huang, H. Sun, D. Shen, M. Wang, J. Hu, Y. Lu, K.-J. Zhou, and D. Feng, Electronic and magnetic excitations in $\text{La}_3\text{Ni}_2\text{O}_7$, [arXiv:2401.12657 \(2024\)](#).
- [76] T. Xie, M. Huo, X. Ni, F. Shen, X. Huang, H. Sun, H. C. Walker, D. Adroja, D. Yu, B. Shen, L. He, K. Cao, and M. Wang, Strong interlayer magnetic exchange coupling in $\text{La}_3\text{Ni}_2\text{O}_{7-\delta}$ revealed by inelastic neutron scattering, *Sci. Bull.* **69**, 3221 (2024).
- [77] E. K. Ko, Y. Yu, Y. Liu, L. Bhatt, J. Li, V. Thampy, C.-T. Kuo, B. Y. Wang, Y. Lee, K. Lee, J.-S. Lee, B. H. Goodge, D. A. Muller, and H. Y. Hwang, Signatures of ambient pressure superconductivity in thin film $\text{La}_3\text{Ni}_2\text{O}_7$, *Nature* **638**, 935 (2025).
- [78] Y. Liu, E. K. Ko, Y. Tarn, L. Bhatt, B. H. Goodge, D. A. Muller, S. Raghu, Y. Yu, and H. Y. Hwang, Superconductivity and normal-state transport in compressively strained $\text{La}_2\text{PrNi}_2\text{O}_7$ thin films, [arXiv:2501.08022 \(2025\)](#).